

<https://doi.org/10.1038/s41612-024-00615-3>

# Strengthened impact of boreal winter North Pacific Oscillation on ENSO development in warming climate

Check for updates

Shangfeng Chen<sup>1</sup>, Wen Chen<sup>2,3</sup>✉, Shang-Ping Xie<sup>4</sup>, Bin Yu<sup>5</sup>, Renguang Wu<sup>6</sup>, Zhibiao Wang<sup>1</sup>, Xiaoqing Lan<sup>1</sup> & Hans-F Graf<sup>7</sup>

The North Pacific Oscillation (NPO), an important mode of atmospheric variability, is a crucial trigger for the development of El Niño–Southern Oscillation (ENSO) via the seasonal footprinting mechanism. How the NPO effect on ENSO changes in response to greenhouse warming remains unclear, however. Here, using climate model simulations under high-emission scenarios, we show that greenhouse warming leads to an enhanced influence of NPO on ENSO as is manifested by enhanced responses of winter sea surface temperature (SST), precipitation and wind anomalies in the equatorial Pacific to the preceding winter NPO. The strengthened NPO impact is also reflected in an increased frequency of NPO events that are followed by ENSO events. Warmer background SST enhances the wind–evaporation–SST feedback over the subtropical North Pacific due to a nonlinear SST–evaporation relationship. This strengthens the NPO-generated surface zonal wind anomalies over the equatorial western-central Pacific, which trigger ENSO. Increased impact of winter NPO on ENSO could enable prediction of interannual variability at longer leads.

El Niño–Southern Oscillation (ENSO) is the strongest air–sea coupling system in the tropics and it exerts substantial impacts on climate, ecosystems, water resources and human livelihoods worldwide<sup>1–7</sup>. Further, ENSO is suggested to be one of the most important sources of seasonal climate predictability in many parts of the world<sup>8,9</sup>. Thus, identifying and understanding the factors relevant to ENSO has been a long-standing issue in climate science.

In addition to the process within the tropical Pacific, recent studies suggested that extratropical ocean–atmospheric variability can influence ENSO on multiple timescales<sup>10–24</sup>. In particular, the boreal winter North Pacific Oscillation (NPO), an important mode of atmospheric variability over the North Pacific<sup>25,26</sup>, can notably influence the following ENSO development via the seasonal footprinting mechanism<sup>10,12,27</sup>. Positive winter NPO-related subtropical cyclonic anomalies lead to sea surface temperature (SST) warming in the subtropical North Pacific via a reduction of upward turbulent heat flux. This winter NPO-generated subtropical SST warming propagates southwestward and induces surface westerly wind anomalies over the equatorial western-central Pacific during the following summer via

the wind–evaporation–SST (WES) feedback<sup>10,12,27</sup>. This further determines the ENSO evolution during the following winter.

Observations showed that the majority of winter NPO events are followed by ENSO events in the following winter, including the strong El Niño events of 1982–83, 1997–98 and 2015–16, and the strong La Niña events of 1988–89, 1998–99, 1999–00 and 2007–08 (Supplementary Fig. 1). Further studies indicated that the enhanced impact of the winter NPO on the tropical Pacific since the early 1990s plays an important role in the recent increased occurrence of central Pacific El Niños, a type of ENSO event with maximum SST anomalies in the tropical central Pacific<sup>28,29</sup>. It is also argued that the extratropical atmospheric variability associated with the NPO is an important source for the occurrence of multi-year El Niño events<sup>30</sup>. Thus, the NPO is an important factor in the generation and complexity of ENSO.

How the influence of the winter NPO on ENSO changes under global warming is an important issue, which contributes to understanding and predicting future ENSO events. This question so far remains unanswered. Using a set of large ensemble climate simulations extracted from the sixth phase of the Coupled Model Intercomparison Project (CMIP6), here we

<sup>1</sup>Center for Monsoon System Research, Institute of Atmospheric Physics, Chinese Academy of Sciences, Beijing, China. <sup>2</sup>Yunnan Key Laboratory of Meteorological Disasters and Climate Resources in the Greater Mekong Subregion, Yunnan University, Kunming, China. <sup>3</sup>Department of Atmospheric Sciences, Yunnan University, Kunming 650500, China. <sup>4</sup>Scripps Institution of Oceanography, University of California, San Diego, La Jolla, CA, USA. <sup>5</sup>Climate Research Division, Environment and Climate Change Canada, Toronto, ON, Canada. <sup>6</sup>School of Earth Sciences, Zhejiang University, Hangzhou, China. <sup>7</sup>Center for Atmospheric Science, University of Cambridge, Cambridge, UK. ✉e-mail: [chenwen-dq@ynu.edu.cn](mailto:chenwen-dq@ynu.edu.cn)

show a strengthened influence of the winter NPO on the subsequent winter ENSO under greenhouse warming.

## Results

### Impact of NPO on ENSO and model evaluations

To obtain the winter NPO pattern, we first apply an EOF analysis on the observed and quadratically detrended D-1JF0 (hereafter time notations of  $-1, 0$  and  $1$  denote preceding, current and following years, respectively) SLP anomalies over the North Pacific ( $20^{\circ}$ – $70^{\circ}$ N and  $120^{\circ}$ E– $100^{\circ}$ W) for the period of 1949–2021. The second EOF mode (EOF2) stands for the NPO pattern (Supplementary Fig. 1). The observed winter NPO index is then obtained by projecting the observed and quadratically detrended D-1JF0 SLP anomalies onto the EOF2. The winter NPO index in the CMIP6 models is obtained using a common basis function approach (Materials and methods): each model's quadratically detrended winter SLP anomalies are projected onto the observed EOF2 to obtain the NPO index in that model. The NPO indices in observations and CMIP6 models are scaled to have a standard deviation (s.d.) of one over the respective full analysis period to depict the temporal variations of the NPO. Regression of SLP anomalies onto the normalized winter NPO index represents the individual spatial patterns of the NPO.

We assess the performance of the 37 CMIP6 models to capture the observed winter NPO in their historical simulations over the period 1900–1990 (referred to as the present-day climate period). The CMIP6 models were able to well simulate the observed spatial pattern of the winter NPO. In particular, the pattern correlations between the D-1JF0 NPO-related SLP anomalies over the North Pacific in the observations and the 37 CMIP6 models are larger than 0.8, although there appears a diversity in the intensity of the southern and northern lobes of the NPO across the models (Supplementary Fig. 2). Furthermore, the majority of the CMIP6 models reproduce reasonably well the seasonality of ENSO, with the monthly variance of the Niño3.4 SST index peaking in boreal winter though there is a diversity of ENSO amplitude in the models (Supplementary Fig. 3).

We examine the correlation coefficient between the D-1JF0 NPO index and the DJF1 Niño3.4 SST index during the present-day climate period to evaluate whether a model is able to reproduce the significant relation between the winter NPO and the following winter ENSO. Hereafter, the D-1JF0 ENSO signal has been removed by means of linear regression to avoid the impact of the ENSO peak signal. A total of 29 models simulate a close relationship of the winter NPO with the following winter ENSO, and these 29 models are selected in the following calculations (Fig. 1a). The multi-model mean (MME) correlation coefficient of the D-1JF0 NPO index with the DJF1 Niño3.4 SST index among the 29 selected models ( $r = 0.28$  with a standard deviation of 0.07) is close to the observed ( $r = 0.31$ ). Furthermore, the MME of the 29 selected CMIP6 models produces well the evolution of the SST and atmospheric anomalies in association with the winter NPO (Fig. 1b–f): A positive D-1JF0 NPO leads to SST warming anomalies in the subtropical North Pacific in spring (Fig. 1c). The generated SST warming anomalies in the subtropical North Pacific propagate equatorward and result in westerly wind anomalies over the tropical western-central Pacific (TWCP) in JJA0 via the WES feedback (Fig. 1d), and contribute to the development of El Niño in the following autumn–winter via the tropical Bjerknes positive air–sea interaction (Fig. 1e, f)<sup>10,12,27</sup>.

### Strengthened impact of winter NPO on ENSO under global warming

We compare the connection of the winter NPO to the following winter ENSO in the 29 selected models between the present-day (1900–1990) and future (2007–2097) climate periods. We calculate the response of the tropical SST anomalies in OND0JF1 to the D-1JF0 NPO. In particular, we regress quadratically detrended OND0JF1 SST anomalies onto the respective normalized D-1JF0 NPO index for the present-day and future climate periods. We then obtain an average of the regression coefficients over the tropical central and eastern Pacific (TCEP,  $5^{\circ}$ S– $5^{\circ}$ N and  $160^{\circ}$ E– $90^{\circ}$ W), yielding the response of the TCEP SST in OND0JF1 to preceding winter

NPO. Most models (25 of the 29 selected models, 86%) generate a strengthened TCEP SST response in OND0JF1 in the future climate (Fig. 2a). The TCEP SST response increases by 32% based on the multi-model mean, from  $0.25^{\circ}$ C in the present-day climate to  $0.33^{\circ}$ C in the future climate (Fig. 2a). This increase passes the 95% confidence level according to the bootstrap test (Figs. 2a, c). When all the 37 CMIP6 models are considered (including 8 models that produce weak NPO–ENSO connection in the present-day climate), a strong inter-model consensus maintains, with 31 of the 37 models generating an increased response (84%, Supplementary Fig. 4). Aggregated over the 37 models, there is an increase of 41%, from  $0.22^{\circ}$ C s.d.<sup>-1</sup> to  $0.31^{\circ}$ C s.d.<sup>-1</sup> (Supplementary Fig. 4).

In addition, the enhanced SST response is associated with an enhanced tropical precipitation response. 26 of the 29 models simulate a strengthened impact of the D-1JF0 NPO on the OND0JF1 precipitation in the TCEP (90%, Figs. 2b, d). The 29-model mean increase is 65%, from  $0.37$  mm day<sup>-1</sup> s.d.<sup>-1</sup> in the present-day climate to  $0.61$  mm day<sup>-1</sup> s.d.<sup>-1</sup> (Fig. 2b). The enhanced impact of the winter NPO on the following winter ENSO is also supported by a comparison between the OND0JF1 SST and wind response patterns between the present-day and future climate periods. Surface westerly wind anomalies and SST warming are stronger in the TCEP under a warmer climate (Figs. 2e, f).

The enhanced impact of the winter NPO results in an increase in the number of NPO events followed by ENSO events. Here, we apply 1.0 s.d. of the D-1JF0 NPO index as a threshold to define the NPO events and 1.0 s.d. of the OND0JF1 Niño3.4 SST index to select ENSO events. The above thresholds of 1.0 s.d. are defined for each of the present-day and future climate periods (instead of the entire analysis period) to avoid the effects of changes in NPO and ENSO amplitude under global warming. We find an increase in the frequency of positive (negative) NPO events followed by El Niño (La Niña) events (Fig. 3). In aggregation, there is a significant increase in the frequency of positive NPO followed by El Niño (22%) from 0.27 under the present-day climate to 0.33 under the future climate (Fig. 3a), and a significant increase in the frequency of negative NPO followed by La Niña (26%) from 0.27 to 0.34 (Fig. 3b). There is also a significant increase in the frequency of winter positive NPO followed by strong El Niño or negative NPO followed by strong La Niña in the future climate (Supplementary Fig. 5). Here, we use 1.5 s.d. of the OND0JF1 Niño3.4 SST index to define strong ENSO events. Aggregated across the 29 models, there is a 39% increase in the occurrence ratio for the positive NPO followed by strong El Niño event, and 22% increase for the negative NPO followed by strong La Niña event under future climate (Supplementary Fig. 5). It should be mentioned that although the MME shows an increase in the occurrence ratio, it is important to point out that about 33% (20%) of the models produce a decrease in the frequency of NPO followed by El Niño (La Niña) events (Fig. 3). This may be because the occurrence of ENSO is also influenced by other extratropical ocean–atmosphere variability in addition to the NPO<sup>10–14,19–23</sup>.

### Increased WES feedback over subtropical North Pacific in a warming climate

Winter NPO-related winds and SST anomalies in the subtropical North Pacific are maintained and propagate southward to the tropical Pacific in the following summer via the WES feedback<sup>10,12</sup>, which further affect the following ENSO development. As in previous studies<sup>15,31,32</sup>, the intensity of the WES feedback is described by the WES parameter, which represents change in the surface latent heat flux induced by per unit change in surface winds (Materials and methods). All 29 models show an enhanced WES feedback over the subtropical North Pacific in MAMJJA0 under a warming climate (Fig. 4a). In response to the similar winter NPO forcing, a stronger WES feedback over the subtropical North Pacific would lead to enhanced JJA0 surface wind anomalies over the TWCP (Fig. 4b), which further exert a stronger impact on the following ENSO (Fig. 2).

Studies have demonstrated that change in the WES feedback is closely related to changes in the background mean surface wind speed and SST<sup>31,32</sup>.

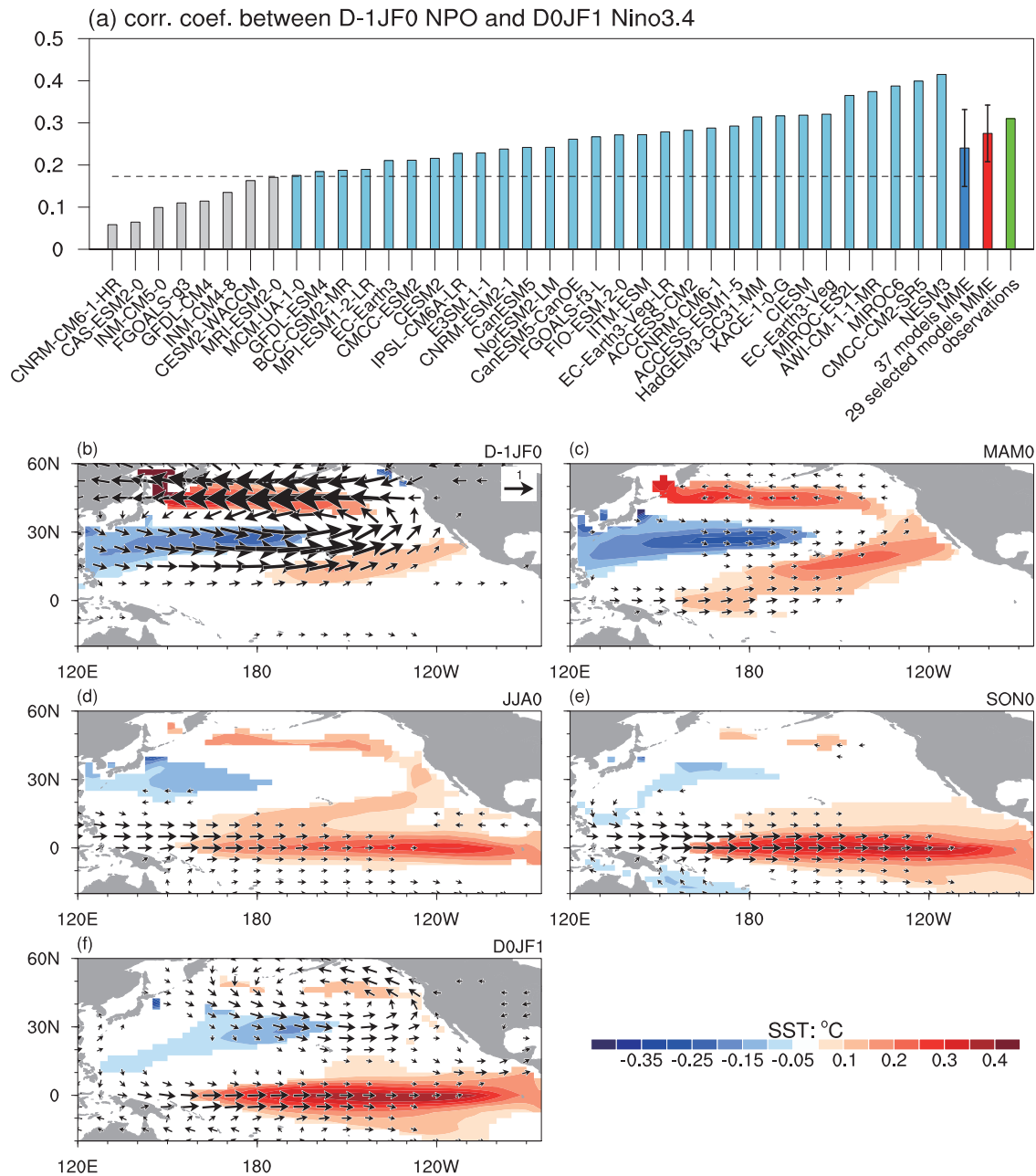


**Fig. 1 | Impact of winter NPO on following ENSO in CMIP6.** **a** Correlation coefficients of the D-1JF0 NPO index and the D0JF1 Niño3.4 SST index over 1900–1990 in 37 CMIP6 models and over 1949–2021 in observations (green bar). Horizontal line in **a** indicates the correlation significant at the 90% confidence level. A total of 29 models can produce significant connection of the D-1JF0 NPO index with the following winter ENSO (light blue bars), thus these 29 models are selected. Dark blue and red bars in **a** indicates multi-model average of the 37 models and the

29 selected models, respectively. Error bars in **a** represent the respective multi-model standard deviation (s.d.) of the considered models. Regression maps of the quadratically detrended SST (°C) and 850-hPa wind ( $m s^{-1}$ ) anomalies in D-1JF0 (**b**), MAM0 (**c**), JJA0 (**d**), SON0 (**e**) and DJF1 (**f**) onto the D-1JF0 NPO index for the multi-model mean of the 29 selected models over 1900–1990. Only ensemble mean of SST anomalies exceeds 1.0 s.d. of the inter-model variation is shown in **b–f**.

On the one hand, stronger background mean surface wind speed will lead to a larger surface latent heat flux response to the same wind anomalies, thus contributing to a stronger WES feedback<sup>31,32</sup>. However, changes in the mean surface wind speed over the subtropical North Pacific are weak (Supplementary Fig. 6), which cannot explain the enhanced WES feedback in the future climate. On the other hand, the WES feedback would be more efficient at a higher background mean SST due to the nonlinear relationship between SST and evaporation<sup>33–35</sup>. Therefore, as suggested by previous studies<sup>18,24</sup>, the enhancement of the WES feedback over the subtropical North Pacific in a warming climate is attributable to a higher background mean SST (Supplementary Fig. 7).

To further confirm that a higher background mean SST contributes to enhanced surface wind anomalies over the TWCP, we perform a set of numerical simulations using the Community Atmospheric Model of version 5.0 of the Community Earth System Model of version 1<sup>36</sup>, including one control experiment and two sensitive experiments. The control experiment is forced by the observed monthly global climatological mean SST (referred to as EXPctrl). The first sensitive experiment (referred to as EXPsnpsst) is forced by observed monthly global climatological mean SST plus winter NPO-generated SST anomalies in MAMJJA0 in the subtropical North Pacific (5°–25°N and 110°–180°W). The second sensitive experiment (referred to as EXPsnpsst&bgsst) is the same as the EXPsnpsst, but

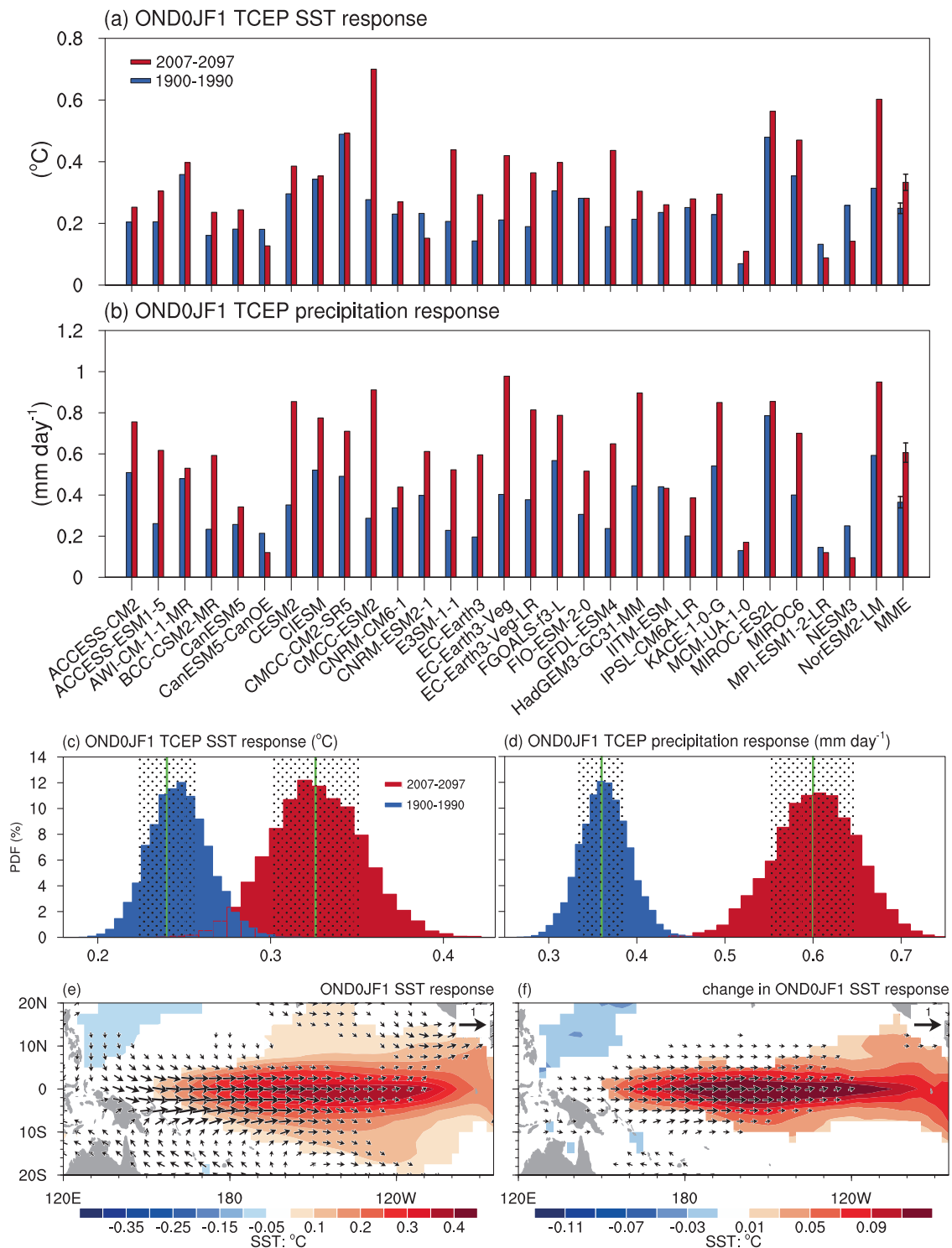


**Fig. 2 | Strengthened impact of winter NPO on following winter ENSO under global warming.** OND0JF1 **a** SST (°C) and **b** precipitation (mm day<sup>-1</sup>) responses in the tropical central-eastern Pacific over the present-day (blue bar) and the future climate period (red bar) in the 29 selected models. Multi-model mean (MME) of the 29 models is also shown in **a**, **b**. Error bars denote 1.0 s.d. of the 10,000 inter-realizations of the bootstrap test (Materials and Methods). Probability distributions of the 10,000 inter-realizations of the **c** OND0JF1 SST and **d** precipitation responses for the present-day (blue bar) and the future climate period (red bar). Green lines in **c**, **d** indicate the mean value of 10,000 inter-realizations, and stippling regions

indicate 1.0 standard deviation of the 10,000 inter-realizations. **e** Regression map of the SST (shading, °C) and 850-hPa wind (m s<sup>-1</sup>) anomalies in OND0JF1 onto the normalized D-1JF0 NPO index for the MME of the 29 selected models over the present-day climate period of 1900–1990. Only MME of SST anomalies exceeds 1.0 s.d. of the inter-model variation is shown in **e**. **f** MME changes in the OND0JF1 SST and 850-hPa wind responses between the future climate period and the present-day climate period for the 29 models. Only the SST changes significantly at the 95% confidence level are shown in **f**.

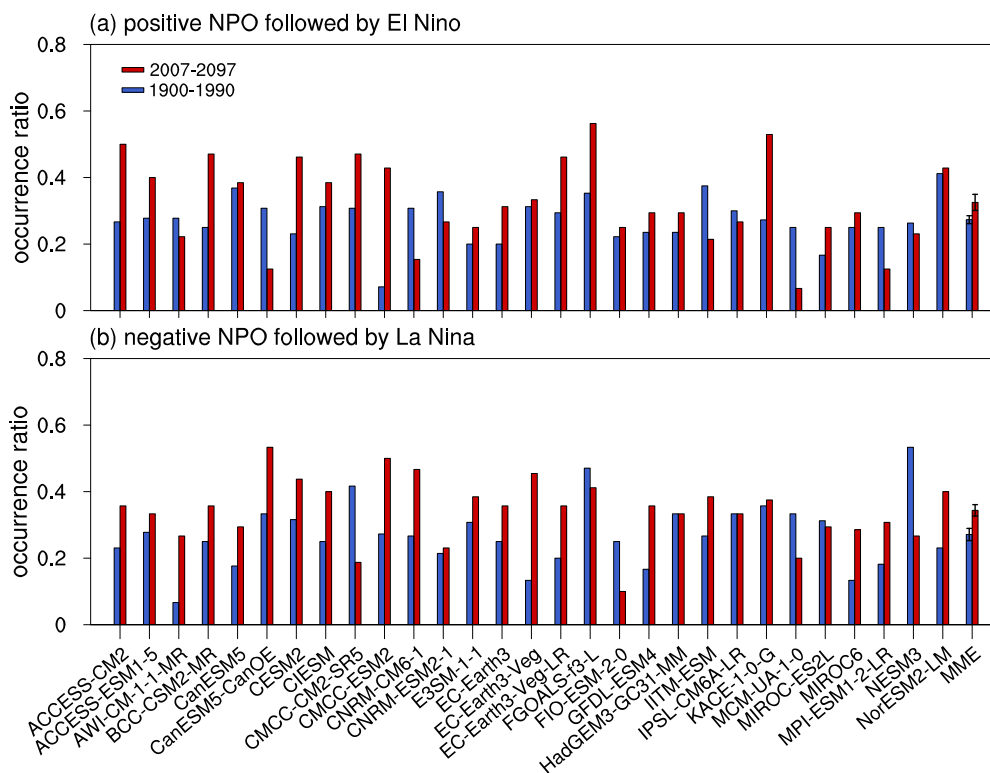


**Fig. 3 | Increased frequency of winter NPO events followed by ENSO events under global warming.** Comparison of the occurrence ratio of **a** positive winter NPO events followed by El Niño events in the following winter over the total positive NPO events, and **b** negative NPO events followed by La Niña events over the total negative

NPO events for the present-day climate period (blue bars) and the future climate period (red bars). The MME and corresponding error bars are also presented. Error bars are defined as 1.0 s.d. of 10,000 inter-realizations of a bootstrap test.

additionally adds the projected background SST warming in spring and summer over the global tropical and subtropical regions (between 40°S and 40°N). A comparison of the EXPsnpsst&bgst and EXPsnpsst provides information about the role of the background SST change. The control experiment is integrated for 40 years, and the two sensitive experiments are integrated for 30 years. The last 28-year means of each experiment are used to access the model response to the SST forcing. It shows that surface westerly wind responses over the TWCP are much stronger in the EXPsnpsst&bgst compared to those in the EXPsnpsst (Figs. 4e, f). This confirms that given the same SST anomalies in the subtropical North Pacific, higher background mean SST could lead to stronger surface wind responses over the tropical Pacific, which further leads to an enhanced influence of winter NPO on ENSO.

Studies have shown that the amplitude of the winter NPO, particularly its southern centre, plays an important role in determining the strength of the winter NPO influence on ENSO<sup>37-39</sup>. We have examined the inter-model relationship between the change in the OND0JF1 TCEP SST response to the D-1JF0 NPO index and the change in the standard deviation of the D-1JF0 NPO index among the 29 CMIP6 models (Supplementary Fig. 8a). The standard deviation of the D-1JF0 NPO index is used to denote the amplitude of the winter NPO. It can be seen from Supplementary Fig. 8a that the change in the winter NPO-ENSO correlation in a warming climate is not related to the change in the winter NPO amplitude. We have also examined the inter-model relationship between the change in the OND0JF1 TCEP SST response to the D-1JF0 NPO and the change in the intensity of the southern centre of the D-1JF0 NPO (Supplementary Fig. 8b). The intensity of the southern lobe of the winter NPO is described by the D-1JF0 SLP anomalies averaged over 20°-45°N and 150°E-130°W regressed on the D-1JF0 NPO index. The two variables in Supplementary Fig. 8b are not closely related with each other. Therefore, the above results together indicate that an increased influence of the winter NPO on the subsequent ENSO in a warming climate is not due to the change in intensity of the winter NPO.

Winter NPO-related subtropical wind stress curl anomalies are able to lead to a charge or discharge of the subsurface ocean heat content in the tropical central Pacific<sup>40-42</sup>. Specifically, positive winter NPO-generated southwesterly wind anomalies over the subtropical North Pacific provide negative surface wind stress curl anomalies over the tropical North Pacific (Supplementary Fig. 9a, b). These negative wind stress curl anomalies lead to downward Ekman pumping and meridional Sverdrup transport toward the tropical central Pacific, which increases the subsurface temperature over the tropical Pacific and is conducive to the El Niño onset. We assess this mechanism by regressing D-1JFM0 surface wind stress curl anomalies over the tropical North Pacific (2.5°-12.5°N and 120°W-180°W-average) onto the normalized D-1JF0 NPO index in the present-day and future climate. Change in the response of the D-1JFM0 surface wind stress curl over the tropical North Pacific between the two periods is weak (Supplementary Fig. 9c). Thus, the enhanced impact of NPO on ENSO is not likely attributed to changes in the trade wind charging mechanism.

Recent studies have indicated that positive winter NPO phase could induce upper-level easterly wind anomalies over the equatorial western-central Pacific in concurrent winter via equatorward wave energy flux, the so-called upper tropospheric process<sup>43,44</sup>. These upper-level easterly wind anomalies could contribute to formation of the low-level westerly wind anomalies in the equatorial western-central Pacific via modulating tropical circulation. Then, the equatorial western-central Pacific low-level westerly wind anomalies further impact the following winter ENSO development<sup>43,44</sup>. We have examined upper-level (200-hPa) zonal wind anomalies in D-1JF0 regressed upon the D-1JF0 NPO index in the present-day and future climate periods for the MME of the 29 CMIP6 models (Supplementary Fig. 10a, b). Positive winter NPO could induce significant upper-level easterly wind anomalies over the equatorial western-central Pacific both during the present-day climate period and the future climate period (Supplementary Fig. 10a, b), consistent with previous findings<sup>43,44</sup>. However, the differences of the upper-level easterly wind anomalies over the equatorial western-

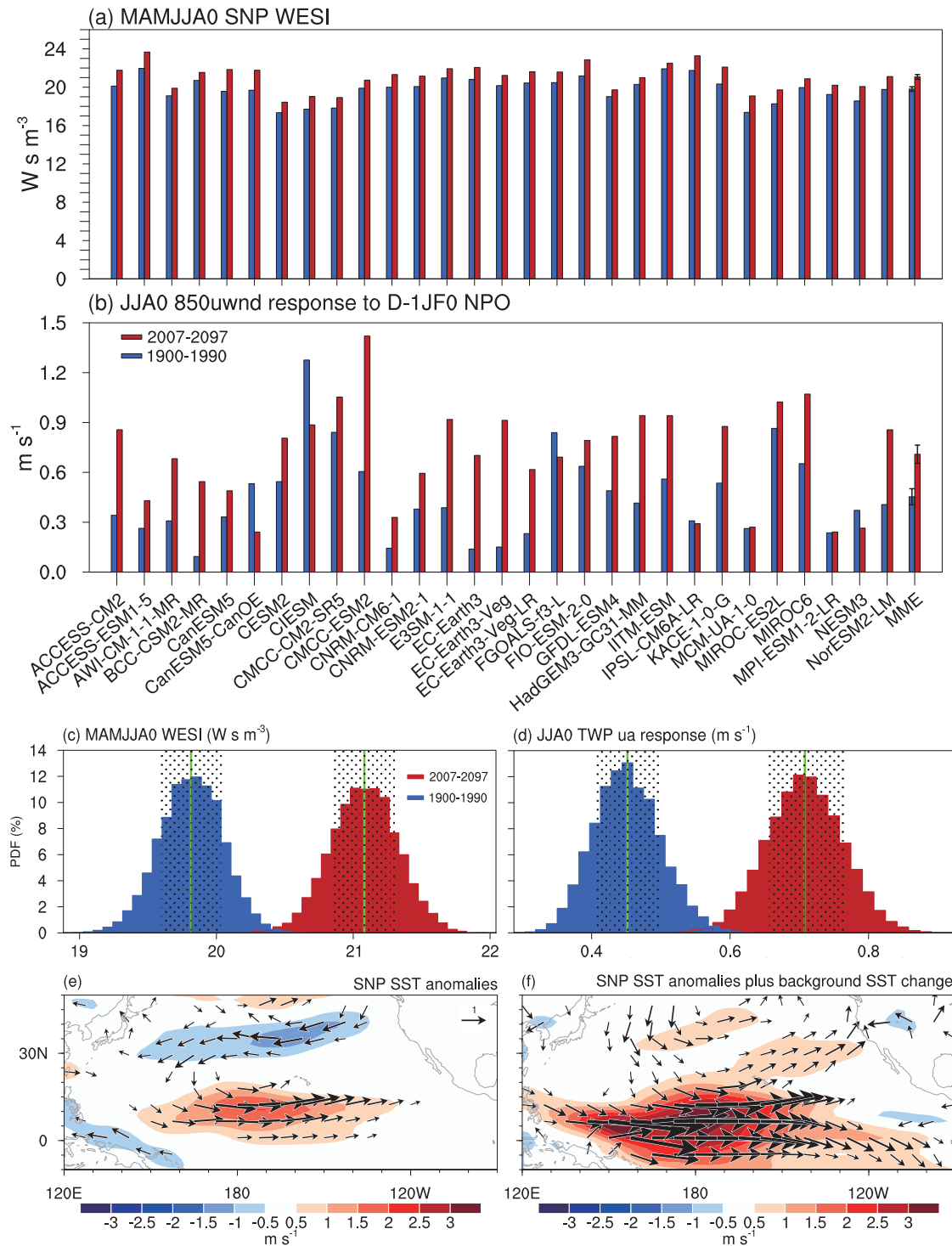


**Fig. 4 | Mechanism for the strengthened impact of winter NPO.** **a** Intensity of the WES feedback (WESI) in MAMJJA0 over the subtropical north Pacific ( $5^{\circ}$ – $25^{\circ}$ N and  $160^{\circ}$ E– $130^{\circ}$ W) during the present-day climate period (blue bars) and future climate period (red bars). **b** JJA0 850-hPa zonal wind anomalies over the tropical western-central Pacific (TWCP,  $5^{\circ}$ S– $5^{\circ}$ N and  $140^{\circ}$ – $180^{\circ}$ E) regressed on the preceding winter NPO index for the present-day climate period (blue bars) and the future climate period (red bars). MME of the models are also shown in **a**, **b**, with error bars denoting 1.0 standard deviation of the 10,000 inter-realizations of the bootstrap test.

Probability distributions of the 10,000 inter-realizations of the **c** MAMJJA0 WESI over subtropical northern Pacific and **d** JJA0 850hPa zonal wind response over TWCP for the present-day climate period (blue bars) and future climate period (red bars). Green lines in **c**, **d** indicate the mean value of the 10,000 inter-realizations, and stippling regions indicate 1.0 standard deviation of the 10,000 inter-realizations. **e** Differences of 850-hPa winds (vectors) and 850-hPa zonal wind (shadings) in JJA0 between the EXPsnpsst and EXPctrl. **f** As in **e**, but for the differences between the EXPsnpsst&bgst and EXPctrl.

central Pacific related to the winter NPO are weak (box region in Supplementary Fig. 10c). This suggests that the intensified impact of the winter NPO on the following ENSO is not due to change of the upper tropospheric process associated with the winter NPO.

**Enhanced impact of NPO on ENSO in large ensemble experiments**

To further confirm the enhanced impact of the winter NPO on the following ENSO, we make use of a set of 100-member experiments from 1950–2100

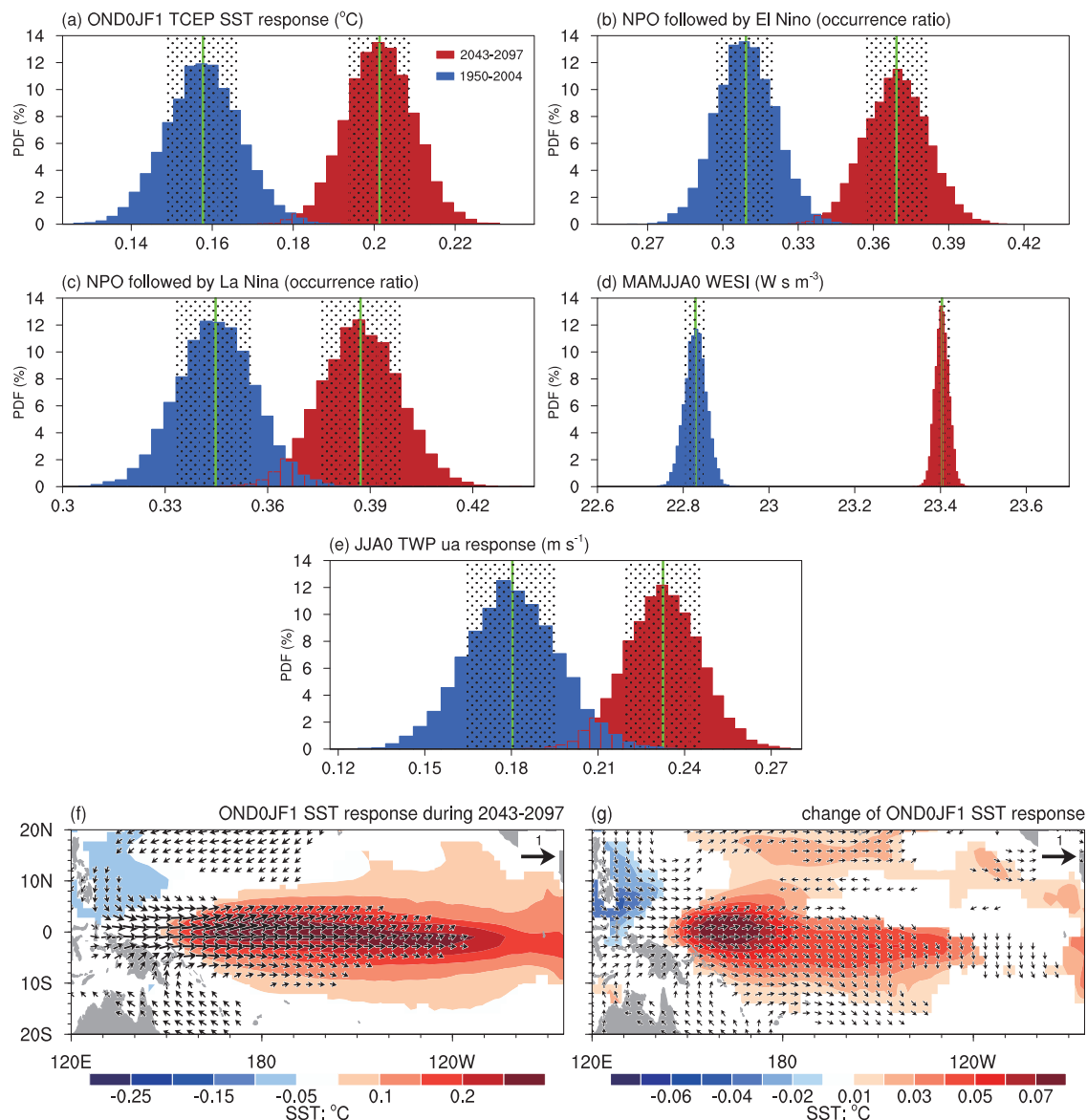


**Fig. 5 | Strengthened impact of winter NPO on ENSO in 100-member large ensemble simulation of MPI-ESM.** **a** Probability distribution of the 10,000 inter-realizations of the bootstrap test for **a** OND0JF1 TCEP SST (°C) response to the D-1JF0 NPO, **b** occurrence ratio of positive D-1JF0 NPO events followed by El Niño events, **c** occurrence ratio of negative D-1JF0 NPO events followed by La Niña events, **d** MAMJJA0 WESI over the subtropical North Pacific, and **e** JJA0 850hPa zonal wind response over the TWCP response to the D-1JF0 NPO for the present-day climate period (blue bars) and future climate period (red bars). Green lines in **a–e** indicate the mean value of 10000 inter-realizations, and stippling regions

indicate 1.0 standard deviation of the 10000 inter-realizations. **f** Regressions of the SST (°C) and 850-hPa wind (m s<sup>-1</sup>) anomalies in OND0JF1 onto the D-1JF0 NPO index for the MME of the 100-member simulations of the MPI-ESM over the future climate period of 2043–2097. Only ensemble mean of SST anomalies exceeds 1.0 s.d. of the inter-member variation is shown in **f**. **g** MME changes in the OND0JF1 SST and 850-hPa wind responses between the future climate period (2043–2097) and the present-day climate period (1950–2004) for the 100-member large ensemble simulation of the MPI-ESM. Only the SST changes significant at the 95% confidence level are shown in **g**.

conducted with the Max Planck Institute for Meteorology Earth System Model (MPI-ESM<sup>45</sup>, Materials and Methods). From 1950 to 2005, the model is forced by historical changes in radiative forcings, including time-varying anthropogenic greenhouse gases, volcanic eruptions, etc. From 2006 to 2100, the model is forced by the RCP8.5 scenario (radiative forcing increases and reaches around 8.5 W m<sup>-2</sup> near 2100). The only differences among the 100-member simulations are slight perturbations in the initial condition. We compare the changes between the two periods: 1950–2004 and 2043–2097. The MPI-ESM simulations capture reasonably well the winter NPO pattern (Supplementary Fig. 11) over the period of 1950–2004. The multi-member ensemble mean also reproduces well the seasonal foot-printing mechanism for the impact of the winter NPO on ENSO (Supplementary Fig. 12). Like in the CMIP6 models, the MPI-ESM experiments

generate an increased correlation between the winter NPO index and the following winter Niño3.4 SST index (Supplementary Fig. 13) and a strengthened OND0JF1 TCEP SST response in most experiments (68%, Fig. 5a, f, g), with a statistically significant increase in the multi-experiment ensemble mean change. The MPI-ESM experiments also produce an increase in the frequency of positive (negative) winter NPO events followed by El Niño (La Niña) events (Figs. 5b, c). Further, as in the CMIP6 models, the WES feedback over the subtropical North Pacific (Fig. 5d) and the summer surface zonal wind response over the TWCP (Fig. 5e) intensity significantly in the MPI-ESM, signifying an enhanced impact of the winter NPO on the following ENSO development under global warming (Fig. 5a).

We have also examined change of the winter NPO-ENSO relation according to the 50-member large ensemble simulations conducted

with the second-generation Canadian Earth System Model<sup>46</sup>. Study has indicated that the CanESM2 can well simulate the physical process for the influence of the winter NPO on the following ENSO<sup>37</sup>. Like in the CMIP6 and the MPI-ESM, the CanESM2 experiments could generate a pronounced enhanced impact of the winter NPO on the following winter ENSO. Particularly, the correlation coefficient between the winter NPO index and the following winter Niño3.4 SST index for the MME of the CanESM2 50 members during the future climate period is significantly larger than that during the present-day climate period (Supplementary Fig. 14). Hence, the above evidences all confirm an enhanced impact of the winter NPO on ENSO in a warming climate.

## Discussion

In conclusion, the impact of the winter NPO on the following winter ENSO becomes stronger under greenhouse warming. In a background of higher mean SST with global warming, the WES feedback over the subtropical North Pacific becomes stronger due to the nonlinear SST–evaporation relationship. The strengthened WES feedback leads to stronger surface zonal wind anomalies over the TWCP in response to the same amplitude of SST anomalies over the subtropical North Pacific induced by the winter NPO, and thus is more conducive to trigger ENSO. The strengthened impact and associated mechanism in CMIP6 models are supported by a set of large ensemble experiments, in which unit change of winter NPO leads to a stronger ENSO-like response under greenhouse warming. This study suggests that winter NPO will become a more influential factor in the development of ENSO as greenhouse warming continues in the future, and thus ENSO may become more predictable if the forecast is initialized in the boreal winter.

ENSO amplitude may change under global warming<sup>47,48</sup>. However, neither the change in the winter NPO–ENSO connection (Supplementary Fig. 15) nor change in the frequency of NPO events followed by ENSO events is related to change in the ENSO amplitude under global warming (Supplementary Fig. 16). A recent study pointed out that the influence of the spring PMM on the following winter ENSO shows an increase under global warming<sup>18</sup>. It is well known that the winter NPO is an important forcing for the formation of the spring PMM. We have examined the response of MAM0 SST anomalies averaged over the subtropical North Pacific (5°–20°N, 180°E–130°W) to the D-1JF0 NPO for the present-day and future climate periods (Supplementary Fig. 17). The regional mean of SST anomalies over 5°–20°N, 180°E–130°W can well represent the spring PMM variability<sup>49,50</sup>. The response of MAM0 SST anomalies over the subtropical North Pacific to the D-1JF0 NPO for the MME of the 29 CMIP6 models is significantly enhanced during the future climate period (Supplementary Fig. 17). Furthermore, there is a close inter-model relationship between the change in the OND0JF1 TCEP SST response to D-1JF0 NPO and the change in the MAM0 SST anomalies over the subtropical North Pacific response to D-1JF0 NPO among the 29 CMIP6 models (Supplementary Fig. 18). This suggests that an enhanced influence of the winter NPO on the following ENSO in a warming climate could be partly attributed to the enhanced influence of the winter NPO on the subsequent spring PMM.

## Methods

### Observational and reanalysis data

Monthly mean SLP, three-dimensional wind velocities, precipitation rate, surface zonal and meridional winds, and surface zonal and meridional momentum fluxes are obtained from the National Centers for Environmental Prediction–National Center for Atmospheric Research reanalysis<sup>51</sup> (NCEP/NCAR), which are available from January 1948 to the present. SLP and three-dimensional velocities from the NCEP/NCAR have a horizontal resolution of  $2.5^\circ \times 2.5^\circ$  in longitude–latitude grids, and other surface variables are on T62 Gaussian grids. Monthly mean SST data are derived from the National Oceanic and Atmospheric Administration (NOAA) Extended Reconstructed SST version 5 (ERSSTv5) dataset<sup>52</sup>, which have a horizontal resolution of  $2.5^\circ \times 2.5^\circ$  and span the time period from January 1854 to the

present. All the observational and reanalysis data are quadratically detrended over the analysis period of 1949–2021.

### CMIP6 data

We examine monthly outputs from the 37 CMIP6 models forced by historical forcing up to 2014 (Historical simulations) and the Shared Socio-economic Pathway 5–8.5 scenario to 2100<sup>53</sup> (SSP5–8.5 simulations) (Supplementary Table 1). Monthly mean sea level pressure, precipitation rate, surface temperature, three-dimensional velocities, surface zonal and meridional winds, and surface zonal and meridional momentum fluxes are all available in the historical and SSP5–8.5 simulations of the 37 CMIP6 models. We employ one member of each model, which is mostly r1i1p1f1 simulation (Supplementary Table 1). To calculate multi-model average and pattern correlations between observed and simulated results, all the data are converted to a common horizontal resolution of  $2^\circ \times 2^\circ$ . All the CMIP6 data are quadratically detrended over the full period of 1900–2100. Monthly anomalies are constructed by removing the monthly mean climatology over the full period of 1900–2099 before they are quadratically detrended. We compare the impact of winter (D-1JF0) NPO on the following winter (D0JF1) ENSO between the two 91-year periods, i.e., present-day climate period (1900–1990) and the future climate period (2007–2097). The 91-year period is used to reduce the influence from internal variability as much as possible.

### Large ensemble simulations

To confirm the results obtained from the CMIP6 models, we also use 100-member large ensemble simulations conducted with the MPI-ESM<sup>45</sup> and 50-member large ensemble simulations conducted with the CanESM2<sup>46</sup>. MPI-ESM is a fully coupled atmosphere–ocean–land–sea ice climate model with a horizontal resolution of about  $1.9^\circ \times 1.9^\circ$  in the longitude–latitude grids. From 1950 to 2005, each of the MPI-ESM simulations is forced by observed historical changes in radiative forcing agents including time-varying anthropogenic sulfate aerosols, greenhouse gases, ozone concentrations, land-use change, and volcanic eruptions, similar to the corresponding CMIP5 simulations. From 2006 to 2100, the MPI-ESM simulations are forced by the representative concentration pathway 8.5 (RCP8.5), where the radiative forcing increases and reaches around  $8.5 \text{ W m}^{-2}$  near 2100. The CanESM2 is also a fully coupled atmosphere–ocean–land–sea ice general circulation model<sup>46</sup>. Regarding the CanESM2, five simulations are firstly performed for the period of 1850–1950 to produce five different oceanic states in 1950. Ten experiments are then run from each of the above five historical simulations with slightly different initial conditions in 1950, generating a total of 50 ensemble members of 150-yr simulations for the period of 1950–2100. The 100-member large ensemble simulations of the MPI-ESM and the 50-member large ensemble simulations of the CanESM2 are forced by the same external forcing with only slight differences in the initial conditions, and thus the diversity of results among the different ensemble members is attributed solely to the internal climate variability.

### Common basis function approach

In place of the NPO usually taken as EOF2 of the North Pacific SLP anomalies, we use the common basis function (CBF) approach<sup>54,55</sup> to extract the NPO pattern. The CBF approach circumvents the problems of conventional EOF analysis. For instance, it avoids the issue that the EOF2 of the model simulation does not always capture the characteristics of the NPO for some models, particularly if the simulated EOFs are not well separated. The CBF approach is performed as follows. First, in the observations, the NPO pattern is represented by the EOF2 of SLP anomalies over the North Pacific ( $20^\circ$ – $70^\circ$ N and  $120^\circ$ – $100^\circ$ W) during 1949–2021. Then, the observed NPO index is calculated by projecting the observed and quadratically detrended winter SLP anomalies onto the aforementioned EOF2 mode over the North Pacific region ( $20^\circ$ – $70^\circ$ N and  $120^\circ$ – $100^\circ$ W). Meanwhile, the NPO index in the 37 CMIP6 models is calculated by projecting the respective quadratically detrended simulated



winter SLP anomalies onto the observed EOF2 pattern over the full period of 1900–2099.

### WES parameter

As in previous studies<sup>15,31,32</sup>, the intensity of the WES is described by the WES parameter, indicating the sensitivity of evaporation at the ocean surface to surface wind changes. The WES parameter can be expressed as follows:

$$\alpha = -\frac{\partial L}{\partial u} = -L \frac{u}{\bar{w}^2}$$

Here,  $\alpha$  is the WES parameter, indicating the sensitivity of evaporation at the ocean surface to surface wind changes.  $L$  represents surface latent heat flux,  $u$  is the surface zonal wind anomaly, and  $\bar{w}$  denotes the mean wind speed.

### Intensity of the NPO's southern and northern lobes

First, we obtain the winter NPO pattern by regressing the quadratically detrended D-1JF0 SLP anomalies onto the normalized D-1JF0 NPO index over the full analysis period. The intensity of the NPO's southern lobe is then defined as D-1JF0 SLP anomalies averaged over 20°–45°N and 150°E–130°W. Meanwhile, the intensity of the NPO's northern lobe is obtained by averaging D-1JF0 SLP anomalies over the region of 50°–80°N and 160°E–120°W.

### ENSO variability

ENSO variability is represented by the boreal winter Niño3.4 SST index, defined by region-mean SST anomalies over 5°S–5°N and 120°–170°W.

### Bootstrap test

We employ a bootstrap test to estimate whether changes in the response of OND0JF1 SST to D-1JF0 NPO index between the present-day and future climate periods are statistically significant<sup>56</sup>. Specifically, we first obtain OND0JF1 SST responses as OND0JF1 SST anomalies averaged in the TCEP by regressions on the normalized D-1JF0 NPO index in the present-day and future climate periods from the 29 selected CMIP6 models, respectively. Then, the OND0JF1 TCEP SST responses in the present-day and future climate periods are resampled randomly to construct respective 10000 realizations. In this random resampling process, results in any models can be chosen again. The standard deviations of the 10,000 inter-realizations of the OND0JF1 TCEP SST response for the present-day and future climate periods are 0.02 and 0.03 °C, respectively. The OND0JF1 TCEP SST responses in the future and present-day climate periods are 0.33 and 0.25 °C, respectively. Thus, the difference of the OND0JF1 SST response between the future and present-day climate periods (0.08 °C) is larger than the sum of the standard deviation in the future and present climate periods (0.05 °C), suggesting that the difference is statistically significant at the 95% confidence level. The bootstrap test method is also used to estimate whether change in the occurrence ratio of winter NPO events followed by ENSO events between the present-day and future climate periods are statistically significant.

### Data availability

Data employed in this study are available from the corresponding authors and can be freely obtained from the following websites: The NCEP-NCAR Reanalysis data are derived from <https://www.esrl.noaa.gov/psd/data/gridded/data.ncep.reanalysis.derived.html>; The ERSSTv5 SST data are derived from <https://psl.noaa.gov/data/gridded/data.noaa.ersst.v5.html>; The CMIP6 historical and SSP5–8.5 simulation outputs are derived from <https://esgf-node.llnl.gov/projects/cmip6/>. The MPI-ESM large ensemble simulations are derived from <https://esgf-data.dkrz.de/projects/mipi-ge/>.

### Code availability

All codes are available from the corresponding author upon reasonable request.

Received: 30 November 2023; Accepted: 4 March 2024;

Published online: 12 March 2024

### References

- Jin, F.-F. Tropical ocean–atmosphere interaction, the Pacific Cold Tongue, and the El Niño–Southern Oscillation. *Science* **274**, 76–78 (1996).
- Wallace, J. M. et al. The structure and evolution of ENSO-related climate variability in the tropical Pacific: lessons from TOGA. *J. Geophys. Res.* **103**, 14241–14259 (1998).
- Neelin, J. D. et al. ENSO theory. *J. Geophys. Res.* **103**, 14261–14290 (1998).
- Cai, W. et al. Butterfly effect and a self-modulating El Niño response to global warming. *Nature* **585**, 68–73 (2020).
- McPhaden, M. J., Zebiak, S. E. & Glantz, M. H. ENSO as an integrating concept in Earth science. *Science* **314**, 1740–1745 (2006).
- Long, Y. Q., Zhang, X. Y. & Mai, B. R. Impact of ENSO on MJO propagation behaviors. *J. Trop. Meteor.* **38**, 410–421 (2022).
- Bi, C. X., Ren, B. H. & Zheng, J. Q. Asymmetric effects Of ENSO on precipitation in the western North Pacific during the following summer. *J. Trop. Meteor.* **39**, 89–101 (2023).
- Webster, P. J. et al. Monsoons: Processes, predictability, and the prospects for prediction. *J. Geophys. Res.* **103**, 14451–14510 (1998).
- Barnston, A. G., Tippett, M. K., L'Heureux, M. L., Li, S. H. & DeWitt, D. G. Skill of real-time seasonal ENSO model predictions during 2002–11 Is our capability increasing? *Bull. Am. Meteor. Soc.* **93**, 631–651 (2012).
- Vimont, D. J., Battisti, D. S. & Hirst, A. C. Footprinting: a seasonal connection between the tropics and mid-latitudes. *Geophys. Res. Lett.* **28**, 3923–3926 (2001).
- Chang, P. et al. Pacific Meridional mode and El Niño–Southern oscillation. *Geophys. Res. Lett.* **34**, L16608 (2007).
- Vimont, D. J., Alexander, M. A. & Newman, M. Optimal growth of central and East Pacific ENSO events. *Geophys. Res. Lett.* **41**, 4027–4034 (2014).
- Yu, J.-Y. & Kim, S. T. Relationships between extratropical sea level pressure variations and the Central-Pacific and Eastern-Pacific types of ENSO. *J. Clim.* **24**, 708–720 (2011).
- Min, Q., Su, J., Zhang, R. & Rong, X. Impact of the South and North Pacific meridional modes on the El Niño–Southern Oscillation: observational analysis and comparison. *J. Clim.* **30**, 1705–1720 (2017).
- Amaya, D. J. The Pacific Meridional Mode and ENSO: a review. *Curr. Clim. Change Rep.* **5**, 296–307 (2019).
- Chen, S. F., Chen, W., Wu, R., Yu, B. & Graf, H. F. Potential impact of preceding Aleutian Low variation on the El Niño–Southern Oscillation during the following winter. *J. Clim.* **33**, 3061–3077 (2020).
- Chen, S. F. et al. Enhanced impact of the Aleutian Low on increasing the Central Pacific ENSO in recent decades. *npj Clim. Atmos. Sci.* **6**, 29 (2023).
- Jia, F. et al. Enhanced North Pacific impact on El Niño/Southern Oscillation under greenhouse warming. *Nat. Clim. Change* **11**, 840–849 (2021).
- Ding, R. Q. et al. Linking the North American dipole to the Pacific Meridional Mode. *J. Geophys. Res.* **124**, 3020–3034 (2019).
- Ding, R. Q. et al. The Victoria mode in the North Pacific linking extratropical sea level pressure variations to ENSO. *J. Geophys. Res.* **120**, 27–45 (2015).
- Ding, R. Q., Li, J. P. & Tseng, Y. H. The impact of South Pacific extratropical forcing on ENSO and comparisons with the North Pacific. *Clim. Dyn.* **44**, 2017–2034 (2015).
- Fan, H. J., Huang, B. H., Yang, S. & Dong, W. J. Influence of the Pacific Meridional Mode on ENSO evolution and predictability: asymmetric modulation and ocean preconditioning. *J. Clim.* **34**, 1881–1901 (2021).

23. Fan, H. J., Wang, C. Z. & Yang, S. Asymmetry between positive and negative phases of the Pacific meridional mode: A contributor to ENSO transition complexity. *Geophys. Res. Lett.* **50**, e2023GL104000 (2023).
24. Fan, H. J., Yang, S., Wang, C., Wu, Y. & Zhang, G. Strengthening amplitude and impact of the Pacific Meridional Mode on ENSO in the warming climate depicted by CMIP6 models. *J. Clim.* **35**, 5195–5213 (2022).
25. Walker, G. T. & Bliss, W. E. World weather V. Memories of the royal meteorological. *Society* **44**, 53–84 (1932).
26. Rogers, J. C. The North Pacific oscillation. *J. Climatol.* **1**, 39–57 (1981).
27. Vimont, D. J., Wallace, J. M. & Battisti, D. S. The seasonal footprinting mechanism in the Pacific: Implications for ENSO. *J. Clim.* **16**, 2668–2675 (2003).
28. Yu, J. Y., Lu, M. & Kim, S. T. A change in the relationship between tropical central Pacific SST variability and the extratropical atmosphere around 1990. *Environ. Res. Lett.* **7**, 034025 (2012).
29. Yeh, S. W., Wang, X., Wang, C. & Dewitte, B. On the relationship between the North Pacific climate variability and the Central Pacific El Niño. *J. Clim.* **28**, 663–677 (2015).
30. Ding, R. Q. et al. Multi-year El Niño events tied to the North Pacific Oscillation. *Nat. Commun.* **13**, 3871 (2022).
31. Vimont, D. J., Alexander, M. A. & Fontaine, A. Midlatitude excitation of tropical variability in the Pacific: the role of thermodynamic coupling and seasonality. *J. Clim.* **22**, 518–534 (2009).
32. Vimont, D. J. Transient growth of thermodynamically coupled variations in the tropics under an equatorially symmetric mean state. *J. Clim.* **23**, 5771–5789 (2010).
33. Seager, R., Naik, N. & Vogel, L. Does global warming cause intensified interannual hydroclimate variability? *J. Clim.* **25**, 3355–3372 (2012).
34. Hu, K., Huang, G., Huang, P., Kosaka, Y. & Xie, S.-P. Intensification of El Niño-induced atmospheric anomalies under greenhouse warming. *Nat. Geosci.* **14**, 377–382 (2021).
35. Liguori, G. & Di Lorenz, E. Meridional modes and increasing Pacific decadal variability under greenhouse forcing. *Geophys. Res. Lett.* **45**, 983–991 (2018).
36. Neale, R. B. et al., Description of the NCAR Community Atmosphere Model (CAM 5.0), Tech. Note 486+STR, Nat. Cent. for Atmos. Res., Boulder, Colorado. (2010).
37. Chen, S. F. & Yu, B. The seasonal footprinting mechanism in large ensemble simulations of the second generation Canadian Earth System Model: Uncertainty due to internal climate Variability. *Clim. Dyn.* **55**, 2523–2541 (2020).
38. Park, J. H. et al. Role of the climatological intertropical convergence zone in the seasonal footprinting mechanism of the El Niño–Southern Oscillation. *J. Clim.* **34**, 5243–5256 (2021).
39. Furtado, J. C., Di Lorenzo, E., Anderson, B. T. & Schneider, N. Linkages between the North Pacific oscillation and central tropical Pacific SSTs at low frequencies. *Clim. Dyn.* **39**, 2833–2846 (2012).
40. Chakravorty, S. et al. Testing the Trade Wind Charging mechanism and its influence on ENSO variability. *J. Clim.* **33**, 7391–7411 (2020).
41. Vimont, D., Alexander, M. & Fontaine, A. Mid-latitude excitation of tropical variability in the Pacific: the role of thermodynamic coupling and seasonality. *J. Clim.* **22**, 518–534 (2008).
42. Anderson, B., Perez, R. C. & Karspeck, A. Triggering of El Niño onset through trade wind-induced charging of the equatorial Pacific. *Geophys. Res. Lett.* **40**, 1212–1216 (2013).
43. Zhao, J. W., Sung, M. K., Park, J. H., Luo, J. J. & Kug, J. S. Part I observational study on a new mechanism for North Pacific Oscillation influencing the tropics. *npj Clim. Atmos. Sci.* **6**, 15 (2023a).
44. Zhao, J. W., Sung, M. K., Park, J. H., Luo, J. J. & Kug, J. S. Part II model support on a new mechanism for North Pacific Oscillation influence on ENSO. *npj Clim. Atmos. Sci.* **6**, 16 (2023b).
45. Maher, N. et al. The Max Planck institute grand ensemble: Enabling the exploration of climate system variability. *J. Adv. Model. Earth Syst.* **11**, 2050–2069 (2019).
46. Sigmond, M. & Fyfe, J. C. Tropical Pacific impacts on cooling North American winters. *Nat. Clim. Change* **6**, 970–974 (2016).
47. Collins, M. et al. The impact of global warming on the tropical Pacific Ocean and El Niño. *Nat. Geosci.* **3**, 391–397 (2010).
48. Cai, W. et al. ENSO and greenhouse warming. *Nat. Clim. Change* **5**, 849–859 (2015).
49. Richter, I., Stuecker, M. F., Takahashi, N. & Schneider, N. Disentangling the North Pacific Meridional Mode from tropical Pacific variability. *npj Clim. Atmos. Sci.* **5**, 94 (2022).
50. Zheng, Y. Q., Chen, S. F., Chen, W. & Yu, B. A continuing increase of the impact of the spring North Pacific Meridional Mode on the following winter El Niño and Southern Oscillation. *J. Clim.* **36**, 585–602 (2023).
51. Kalnay, E. et al. The NCEP/NCAR 40-Year Reanalysis Project. *Bull. Am. Meteor. Soc.* **77**, 437–471 (1996).
52. Huang, B. et al. Extended Reconstructed Sea Surface Temperature version 5 (ERSSTv5), Upgrades, validations, and intercomparisons. *J. Clim.* **30**, 8179–8205 (2017).
53. Eyring, V. et al. Overview of the Coupled Model Intercomparison Project Phase 6 (CMIP6) experimental design and organization. *Geosci. Model. Dev.* **9**, 1937–1958 (2016).
54. Lee, J. et al. Quantifying the agreement between observed and simulated extratropical modes of interannual variability. *Clim. Dyn.* **52**, 4057–4089 (2019).
55. Aru, H. S., Chen, W. & Chen, S.-F. Is there any improvement in simulation of the wintertime Western Pacific Teleconnection pattern and associated climate anomalies in CMIP6 compared to CMIP5 Models? *J. Clim.* **34**, 8841–8861 (2021).
56. Austin, P. C. & Tu, J. V. Bootstrap methods for developing predictive models. *Am. Stat.* **58**, 131–137 (2004).

## Acknowledgements

This work is supported by the National Natural Science Foundation of China (Grants 42175039, and 42230605) and the Natural Science Foundation of Yunnan Province (202302AN360006). We acknowledge the World Climate Research Programme, which, through its Working Group on Coupled Modelling, coordinated and promoted CMIP6. We thank the climate modelling groups for producing and making available their model output, the Earth System Grid Federation (ESGF) for archiving the data and providing access, and the multiple funding agencies that support CMIP6 and ESGF.

## Author contributions

Conceptualization: S.F.C., W.C. Methodology: S.F.C., W.C., S.P.X. Investigation: S.F.C. Visualization: S.F.C., Z.B.W., X.Q.L. Supervision: S.F.C., W.C., S.P.X., B.Y., R.W., H.F.G. Writing—original draft: S.F.C. Writing—review & editing: All the authors.

## Competing interests

The authors declare no competing interests.

## Additional information

**Supplementary information** The online version contains supplementary material available at <https://doi.org/10.1038/s41612-024-00615-3>.

**Correspondence** and requests for materials should be addressed to Wen Chen.

**Reprints and permissions information** is available at <http://www.nature.com/reprints>

**Publisher's note** Springer Nature remains neutral with regard to jurisdictional claims in published maps and institutional affiliations.

**Open Access** This article is licensed under a Creative Commons Attribution 4.0 International License, which permits use, sharing, adaptation, distribution and reproduction in any medium or format, as long as you give appropriate credit to the original author(s) and the source, provide a link to the Creative Commons licence, and indicate if changes were made. The images or other third party material in this article are included in the article's Creative Commons licence, unless indicated otherwise in a credit line to the material. If material is not included in the article's Creative Commons licence and your intended use is not permitted by statutory regulation or exceeds the permitted use, you will need to obtain permission directly from the copyright holder. To view a copy of this licence, visit <http://creativecommons.org/licenses/by/4.0/>.

© The Author(s) 2024